Test of a Large Scale Prototype of the *DIRC*, a Čerenkov Imaging Detector based on Total Internal Reflection for *BaBar* at PEP-II

Colorado State University
H. Staengle, D. Warner, R. Wilson

CEA, DAPNIA, CE-Saclay
R. Aleksan, P. Besson, Ph. Bourgeois, A. de Lesquen, S. Emery, A. Gaidot, L. Gosset, G. Hamel de Monchenault, G. London, E. Pasquetto, D. Therville, G. Vasseur, Ch. Yèche, M. Zito

LAL Orsay
M. Benkebil, R. Cizeron, A. Jouenne, A.M. Lutz, J.M. Noppe, S. Plaszczynski, M.H. Schune, S. Sen, E. Torassa, G. Wormser

Lawrence Berkeley National Laboratory
L. Amerman, D. Brown, A. Ciocio, J. Kadyk, M. Long, G. Lynch, W. Pope, M. Pripstein, G. Przybylski, J. Rasson, J.D. Taylor, T.F. Weber, W. Wenzel

LPNHE des Universités Paris 6 et Paris 7
J. Chauveau, L. del Buono, O. Hamon

LPNHE de l'Ecole Polytechnique, Palaiseau
G. Bonneaud, G. Vasileiadis, M. Verderi

Stanford Linear Accelerator Center
D. Aston, H. Kawahara, H. Krueger, D. McShurley, B.N. Ratcliff, R. Reif, X. Sarazin, J. Schwiening, S. Shapiro, P. Stiles, J. Va'vra

University of British Columbia
C. Hearty

University of California, Santa Barbara
D. Hale, A. Lu

University of Cincinnati
B. Meadows, M. Sokoloff

Abstract

The principles of the DIRC ring imaging Čerenkov technique are briefly explained and its choice for the *BaBar* detector particle identification system is motivated. A large scale prototype of the DIRC for the *BaBar* experiment is then described. Details of the design of this prototype and its test in a hadronic particle beam at the CERN-PS are presented, and results from various prototype and test configurations are given. For example, after correcting for geometrical acceptance and estimated collection effects, the number of photoelectrons was measured to be $146 \pm 1.8 \pm 9\,\mathrm{cm}^{-1}$, for a track angle of 20° at zero photon transmission distance. The effective attenuation loss was measured to be $4.1 \pm 0.7\%$ per meter of bar length, and the observed single photon resolution was $10.0 \pm 0.2\,\mathrm{mrad}$. This performance is consistent with what was expected from earlier tests and Monte Carlo simulations, and will be fully adequate for the physics demands of the *BaBar* experiment.

1 Introduction

A new type of detector for particle identification will be used in the *BaBar* experiment at the SLAC B Factory (PEP-II). This barrel region detector is called DIRC, an acronym for **D**etection of **I**nternally **R**eflected **Č**erenkov (light). This section briefly describes the DIRC as it will be constructed and used at *BaBar*, motivating the prototype and tests that are the subject of the rest of this article.

1.1 Particle Identification at *BaBar* and PEP-II

PEP-II is an asymmetric e^+e^- collider, with beam energies of 9 upon 3.1 GeV [1]. *BaBar* is the detector dedicated to observing the collisions at PEP-II, with a primary physics goal of observing CP violation in the $B^0\overline{B}^0$ system [2]. *BaBar* is expected to begin taking data early in 1999.

The identification of charged particles as pions, kaons, or protons will be of utmost importance for the primary physics goal of detecting CP violation. Particle identification (PID) will be needed both to reconstruct one of the two B mesons in an exclusive decay mode, and to 'tag' the beauty content of the recoiling B meson (identify it as either a B^0 or a $\overline{B}^0$ when it decayed). To satisfy these needs, the *BaBar* particle identification system must fulfill the following requirements:

- Efficient B meson tagging requires good kaon identification up to momenta of about 2.0 GeV/c. In addition, the rare decay processes $B^0 \to \pi^+\pi^-$ and $B^0 \to K^+\pi^-$ are important for the study of CP violation in *BaBar*. To distinguish these two-body decay modes, the particle identification system must be able to separate pions from kaons for momenta up to about 4.0 GeV/c at large dip angles in the laboratory frame (*i.e.* in the forward direction).
- The PEP-II beams will collide about every 4 ns, and the expected trigger rates and integrated backgrounds are large. Therefore, the particle identification device must be relatively fast and tolerant of backgrounds.
- A calorimeter capable of very good energy resolution will surround the *BaBar* particle identification system. This calorimeter must detect low energy photons with good efficiency in order to reconstruct neutral pions, another crucial ingredient in B meson reconstruction. The incremental volume of material necessary to construct this calorimeter scales roughly linearly with the physical thickness of the PID system. To achieve the best calorimeter performance and to minimize its cost, the PID system must therefore be thin and uniform in both radiation length and physical dimension.

Simulations and early tests of the DIRC indicated that it was capable of satisfying all of these requirements. The full scale prototype described in this note was constructed to refine the performance estimates, and to gain experience in construction and exploitation of this novel device. The DIRC was officially selected as the *BaBar* barrel particle identification system shortly before this prototype was completed.

1.2 The DIRC Concept

Charged particle identification is commonly performed by measuring the speed of a particle. The particle mass (and hence its identity) is determined through relativistic kinematics by combining this speed with an independent measurement of the particle's momentum. Particle speed can be measured directly in time-of-flight systems, or indirectly using the speed dependence of various particle interactions with bulk matter. The DIRC, as well as other particle identification devices, uses Čerenkov radiation [3], exploiting the particle speed dependence of the opening angle of the produced light cone.

A traditional Čerenkov-based particle identification detector is the proximity-focused RICH [4]. In these detectors, Čerenkov light is generated in a thin radiating medium and emerges as a cone around the particle trajectory. The photon detector lies along the particle path and must be sufficiently far away from the radiator to provide adequate angular resolution. Some Čerenkov light is trapped in the radiator due to total internal reflection, which reduces the effectiveness of this type of device when particles intersect the radiator surface obliquely.

In the DIRC concept [5], this traditional method of detecting Čerenkov photons is inverted, with the photons transmitted through the radiator being lost, while those trapped in the radiator due to total internal reflection being detectable. This is shown schematically in figure 1. The DIRC radiator is a long, straight bar with a rectangular cross section. Once generated, the Čerenkov light is transported through successive total internal reflections to the ends of the radiator bars. Since the cross-section is rectangular, reflections at the surfaces of the bar preserve the magnitude of the Čerenkov angle at which the photon was produced, but add up-down and left-right ambiguities. The DIRC's effectiveness increases with the steepness of the particle incident angle, as more light is both generated and trapped at steeper angles, matching well with the specific needs of *BaBar*.

To maximize the fraction of trapped light, the bar is made from a material with a high refractive index, typically fused silica (quartz), and is held in an environment with low refractive index, typically air or nitrogen. Quartz is a good choice for the bar material due to its high refractive index, low chromatic dispersion, long radiation length, long volume absorption length for near UV light, and because it can be given a high quality optical finish.

Depending on the particle incident angle, Čerenkov light trapped in the DIRC bar will be reflected to either one or both bar ends. To avoid having to instrument both bar ends with photon detectors, a mirror is placed at one end, perpendicular to the bar axis. This mirror returns most of the incident photons to the other (instrumented) bar end. The bar end mirror preserves the Čerenkov production angle at the cost of an additional ambiguity. This front-back ambiguity can generally be resolved by measuring the photon arrival time.

Most of the photons exit the bar when they reach the instrumented end, and the Čerenkov image is then allowed to expand. The expansion medium is chosen to have a refractive index which approximately matches that of the bar, in order to minimize the total internal reflection at their interface. Purified water is a good choice for the expansion medium because of its high refractive index, its reasonable cost, and its large absorption length in the Čerenkov light wavelengths accessible to photomultiplier tubes (PMTs). The wavelength dependence of water's refractive index also matches well with that of quartz, giving a small chromatic dispersion to the light refraction at their interface. This region containing the water is called the Standoff Box (SOB).

Photons are detected on a two-dimensional surface outside the particle-sensitive volume of the detector. Detection is performed by PMTs. The expected Čerenkov light pattern at this surface is essentially a conic section, whose cone opening angle is the Čerenkov production angle modified by refraction as it emerges from the bar end. The conic section image would be doubled because of the up-down reflection ambiguity, except that a mirror is used to reflect the lower arc onto the upper one. This mirror is slightly tilted, to minimize the displacement of the reflected image due to the finite bar thickness.

The left-right reflection ambiguity, however, does produce a double image, except when the particle incident angle is normal to the surface in the transverse projection. In the general case, the DIRC Čerenkov image consists of two conics tilted with respect to each other by twice the magnitude of the transverse incidence angle. External measurement of this angle by a tracking chamber will allow these images to be combined during Čerenkov angle reconstruction.

A further reduction in the area requiring instrumentation can be made by reflecting the Čerenkov light emitted from the bar at large angles back into a more central range. This reflection adds another ambiguity, which can generally be resolved by pattern recognition during Čerenkov angle reconstruction.

Preliminary tests of the DIRC concept were made in 1993-1994 [6]. These tests used a 2.4 m long bar with a hardened cosmic-muon beam. Čerenkov photons were detected either by a single phototube glued to the bar end (to measure the total photoelectron rate), or by a small array of phototubes suspended in air at varying distances up to 90 cm from the bar end to measure the angular resolution, and these results were compared with simulations. Input to the simulation included an estimate of the PMT spectral response provided by the manufacturer, and known transmission properties of the materials involved. These tests measured a Čerenkov quality factor N_0 at zero transmission distance of $150\,\mathrm{cm}^{-1}$, and a photon attenuation of $8.5 \pm 0.6\%$ per meter of bar length. An angular resolution corresponding to 10 ± 1 mrad in water was also measured. These results were consistent with simulations.

1.3 The DIRC for *BaBar*

The *BaBar* detector is shown schematically in an elevation view section in figure 2. It is built around a solenoidal magnet, and thus has a cylindrical central barrel region. The DIRC bars will be arranged as a 12-sided polygonal barrel between the drift chamber and the crystal calorimeter. Each side of the polygon will consist of 12 bars placed very close together ($75\,\mu$m gap) side by side, for a total of 144 bars.

In the present design the bars have transverse dimensions of 1.7 cm thick by 3.5 cm wide, and are about 4.90 m long. The length is achieved by gluing end-to-end four 1.225 m bars, that size being the longest high quality quartz bar currently available from industry.

The mirrors in the Standoff Box described in section 1.2 have recently been replaced in the *BaBar* DIRC design by a quartz 'wedge' which is glued to the signal end of each bar. The wedge is a 9 cm long block of quartz with the same width as the bars (3.5 cm), and a trapezoidal profile (2.8 cm high at the bar end and 8 cm high at the quartz window which provides the interface to the water). Total internal reflection on all sides of the quartz wedge provides nearly lossless reflection, thereby increasing the number of detectable photons relative to the mirror design. The wedge design also slightly improves the angular resolution, allows a stronger and more robust water seal, and eliminates the need for post-installation alignment of the mirrors.

The DIRC will occupy 8 cm of radial space including supports and construction tolerances. The bars will cover 94% of the azimuthal angle, 87% of the center-of-mass polar angle ($\cos\theta$), and present approximately 14% of a radiation length to normal incident particles. Mechanical support materials in the active region contribute about another 5% of a radiation length to particles at normal incidence.

Because of the beam momentum asymmetry, the center-of-mass polar angle distribution is compressed in the laboratory forward direction, and expanded in the backward direction. To minimize the interference with other detector systems in the crowded forward region, the DIRC instrumented end will be in the backward direction.

Thick barrel end-caps are needed to return the solenoid's magnetic flux. The DIRC bars will extend through this steel to bring the Čerenkov light outside the active and magnetic volume. To maintain at least 95% of their nominal efficiency, the PMTs must be kept in a region free from transverse magnetic fields stronger than about 2 Gauss. A steel enclosure around the Standoff Box together with a bucking coil mounted on *BaBar* near the beam-line will be used to keep the fringe field from the solenoid below this level over the full active surface.

The relatively small aspect ratio of the DIRC (length to diameter) allows a cantilevered mechanical support to be used. The cantilever will be supported in the iron end-cap region by a thick steel tube, which also helps to minimize the magnetic flux gap caused by the quartz bars. The bars will be supported in the active region by a thin extension of this tube. This active volume support tube will be made of thin aluminum inner and outer shells covering an aluminum frame. The frame will be made of thin-wall bulkhead rings spaced every 60 cm along the tube axis. The space between the bulkheads will be filled by construction foam. There will be no DIRC mechanical supports in the forward end of *BaBar*, minimizing its impact on the other detector systems located there.

The *BaBar* DIRC will use 2.82 cm diameter PMTs constructed by Thorn EMI [7]. These tubes have high gain and good quantum efficiency (around 25%) in the Čerenkov wavelengths transmitted by both quartz and water, and are available at modest price. These will be arranged in a nearly close-packed hexagonal pattern on the detection surface. Hexagonal light concentrators on the front of the PMTs will result in an effective active surface area fraction of approximately 90%.

The PMTs will lie on a surface that is approximately toroidal. The distance traversed in the water by the photons emerging from the bar end will be 1.17 m. This distance, together with the size of the bars and PMTs, gives a geometric contribution to the single photon Čerenkov angle resolution of 7 mrad. This geometric contribution is approximately equal to the resolution contribution coming from the production and transmission dispersions.

More information on the *BaBar* DIRC, including performance estimates for pion/kaon separation, can be found in [2].

2 The DIRC Prototype II

While early tests and simulations of the DIRC concept showed promise, many issues remained to be resolved before a DIRC detector for *BaBar* could be designed. The DIRC Prototype II detector was constructed to address these concerns. It was completed in April 1995, and was tested briefly in a hardened cosmic muon beam at LBL. Shortly thereafter, the detector was shipped to CERN where it was tested in a particle beam over a 12 month period. The detector was modified many times in the course of these tests, both to improve the performance of the prototype and to test new schemes for the *BaBar* DIRC. This remainder of this paper describes the original Prototype II plus those modifications which have direct relevance to the performance results presented. Only CERN beam-test results will be presented in this paper.

2.1 The Goals of the Prototype II Tests

The general concerns which Prototype II was intended to address were:

- To refine the early performance estimates;
- To explore the engineering issues associated with constructing a large DIRC detector;
- To gain experience in the long-term operation of a large DIRC detector;
- To provide a test-bench for new ideas as the design of the *BaBar* DIRC proceeded;

The principal specific goals of Prototype II were:

- To observe nearly complete single-particle Čerenkov rings with a water-filled standoff region;
- To measure the photoelectron yield;
- To refine the measurement of photon attenuation due to bar transmission and potential light loss at the glue joint;
- To measure the single photon Čerenkov angle resolution as a function of the position and angle of incident particles;
- To measure the single photon Čerenkov angle resolution as a function of the photon position within the Čerenkov ring;
- To use identified pions and protons in the beam to directly measure the particle identification performance of a DIRC;
- To measure the photon arrival time resolution, and study its use in pattern recognition and background rejection;
- To study the sensitivity of a DIRC to cosmic ray, beam-induced, and intrinsic backgrounds;

- To study potential light cross-talk between side-by-side bars;
- To test the functioning of different calibration systems;
- To achieve a reliable and robust containment of several tons of water;
- To achieve and maintain a large attenuation length for Čerenkov wavelength light in the water;
- To achieve secure and non-damaging mechanical support for the quartz bars;
- To test the operating performance of PMTs immersed in water;
- To evaluate the performance of light concentrators.

2.2 Mechanical Components of Prototype II

The Prototype II consisted of three major mechanical assemblies (see figure 3):

- One or two quartz bars inside a protective box. The bars were coupled to the Standoff Box through a small quartz entrance window.
- A Standoff Box to hold the water, with its mechanical support. This assembly included a small quartz window interface where Čerenkov light from the bar entered the Standoff Box, and a three by three array of nine large quartz windows which allowed the light to pass through to the PMTs after image expansion.
- An array of PMTs. These were optically and mechanically coupled to the Standoff Box exit windows through a thin UV-clear silicone rubber sheet.

For economic reasons, the full image plane of Prototype II could not be instrumented. Instead, a sufficient number of PMTs were purchased to allow covering the Čerenkov ring associated with a single particle incident angle. Separating the PMTs from the water by exit windows allowed re-arranging the PMTs to cover different particle incident angles without draining the water. The segmentation into nine windows facilitated the manufacturing and handling, and allowed some flexibility in testing different PMT mounting arrangements. In particular, one window was later replaced with a jig which held the PMTs directly in the water. A photograph of the prototype during the CERN beam tests is shown in figure 4.

2.2.1 Quartz Bars

The bars were made from an optical grade vitreous fused silica obtained from natural silicon dioxide [8]. The raw material was obtained in large cylindrical ingots 7.6 cm in diameter by 245 cm long. Measurements of the bulk attenuation length with a He-Cd laser indicated a typical light loss of about 3% per meter at 325 nm and about 1% per meter at 442 nm. Six

4.73 cm by 1.7 cm by 120 cm bars were formed from each of these ingots using modifications of conventional optical processing techniques [9]. In general form, the bars produced were rectangular blocks polished on all six sides. In order to preserve the photon angles during surface reflections and to allow a good mechanical fit in the bar box, the faces and sides were nominally parallel while the orthogonal surfaces were kept nominally perpendicular. Typically, the bar's surfaces were flat and parallel to about 0.025 mm, while the orthogonal surfaces were perpendicular to a tolerance of 0.3 mrad. The most difficult requirements were associated with maintaining the photon transmission during reflections at the surfaces of the bar. This led to rather severe requirements on edge sharpness and surface finish, which were met using a large (12 foot diameter) continuous polishing machine. After polishing, the bars had an average edge radius less than 0.005 mm, and a nominal surface polish of better than 0.5 nm root mean squared.

In principle, the surface finish determined the internal reflection coefficient. In practice, this was modified by additional effects, most particularly the surface cleanliness. Even though care was exercised during bar handling and construction, the bars did become dirty after sitting under normal laboratory conditions, and required cleaning. The bars were cleaned with a number of solvents (water, ethanol, acetone, xylene) using drag-wiping followed by flushing and drying with clean N_2 gas. The 0.5 nm surface finish specification corresponds to a predicted internal reflection coefficient of about 0.9999 at 442 nm near 45 degree incidence. Direct measurements of the reflection coefficient with laser light to the required precision were difficult, but typically gave internal reflection coefficients of about 0.9997 at 442 nm with bars that had been recently cleaned [10].

For most of the results presented in this paper, Prototype II was configured with a 2.4 m long bar, which was made from two 1.2 m long bars glued end to end with UV-transmitting epoxy [11]. The area around the joint was carefully cleaned of excess glue in order to minimize the loss of useful surface area.

Another configuration had two 1.2 m bars mounted side by side and parallel, with a 75 μm air gap between then. The bars were attached to the Standoff Box as described below, allowing both to transmit Čerenkov photons into the Standoff Box. This configuration was used to test for light cross-talk between adjacent bars, as described in section 6.8.

2.2.2 Bar Box

The quartz radiator bars were housed inside a rectangular bar box which provided support, and prevented dust and outside light from entering the system. The box was assembled from two aluminum parts with L-shaped cross sections, which allowed the radiator bar to be installed without sliding. The box material was thinned in the regions where the beam penetrated to minimize interactions and scattering. Five adjustable nylon buttons supported the quartz bar at locations designed to minimize the stress on the glue joints. The contact area of the supports was minimized to avoid light loss.

A thin rectangular window (7 cm long by 3.5 cm high by 0.4 cm thick) made from the same raw material as the bars was glued to one end of the bar. It was sealed into a window frame using RTV glue [12]. The bar box was coupled to the water tank through a compliant rubber diaphragm [13] attached to this frame (see figure 5).

The quartz bar was spring loaded with a force equal to the weight of the bar, from the end of the bar box farther from the Standoff Box, to keep the glue joints under compression. The force was applied through the bar end mirror. This mirror had an over-coated aluminum front surface. The mirror was not optically coupled to the bar end, allowing a small air gap between them. This configuration was believed to give the largest net reflectivity, as some of the Čerenkov light was able to reflect nearly losslessly through total internal reflection.

2.3 Standoff Box and Water

The Standoff Box was made of 3/8-inch thick welded aluminum plate with reinforcements, and contained a volume of 1800 liters, 30% of the *BaBar* DIRC volume. The Standoff Box was shaped roughly as an equilateral prism with triangular sides of 1.2 meters and a length of 2.4 meters. This geometry held the image plane 1.2 meters from the bar end at the closest point, inclined at 30° relative to the bar axis. The light opening angle of the Standoff Box was 60°.

The triangular symmetry was broken by a narrow surface truncating one of the long edges. A central port on the narrow surface provided attachment for the bar box. An auxiliary port on this same surface was used for observation, and for calibration devices. To prevent electrolysis, bolts that were in the water were gold plated. Water spigots for filling and draining were provided in several locations.

The bottom of the Standoff Box held a plane glass mirror with front-surface aluminum and dielectric coatings [14]. The mirror was supported by three pads whose heights were adjustable from outside the water volume.

The back plane of the Standoff Box was made from a reinforced lattice made of welded and machined aluminum which could be removed as a unit. It was face-sealed to the rest of the Standoff Box by a flange with a large flat gasket. This lattice held the exit windows, and provided structure for supporting the PMTs.

The nine exit windows (78.9 cm wide by 35.7 cm high by 2.0 cm thick) mounted on the back plane were made from the same raw material as the bars. They were glued into aluminum frames using RTV to make a water-tight seal. The window and frame assemblies were bolted to the back plane. An O-ring between the frame and the back plane flange provided the water seal. These windows defined the image plane of Prototype II.

CERN provided ultra-pure water for the beam tests. The water was changed immediately before each beam run, and was not changed or cleaned during the run period (one to two weeks). Its cleanliness probably degraded slightly with time, but quantitative transmission measurements were not made during the tests.

2.4 Phototubes and Mounting

Hamamatsu model R268 PMTs were chosen to instrument Prototype II because of their small size, their high quantum efficiency, and because they have reasonable timing resolution

[15]. The 456 selected tubes were chosen to have high gain and good stability in laboratory tests.

The PMTs were bundled together mechanically and electrically into groups of 24. Tubes were sorted such that all tubes in a bundle had approximately the same gain when operated at a single voltage. The tubes were run at a gain of the order of 10^8. A custom-built card distributed a common high voltage to all tubes in a bundle, and collected their signals on a multi-pin connector. Raw tube signals were sent through roughly 30 meters of coaxial cable to the amplifiers, resulting in about 30% signal loss at the amplifiers.

The bundles were mechanically assembled from eight triplets of tubes. The triplets were glued together using RTV, with a threaded stainless steel rod glued between them. The eight triplets were held together by bolting the rods to a thick backing plate with appropriately-positioned holes to hold the tubes in a close-pack hexagonal array.

The bundles were attached to the Standoff Box exit windows through 3 mm thick pads of UV-transparent rubber [16]. The bundles were held against the rubber pads by set screws in the Standoff Box back plane which pushed against the backing plate. A force of about five pounds per bundle was needed to eliminate most of the air gaps between the tubes and the rubber sheet. The positions of the bundles on the quartz back windows were established by plastic templates, which touched the tubes on two or three sides of the bundles. The templates (and hence the bundles) could be positioned, with a precision better than 1 mm, over most of the quartz window. Usually, the bundle positions were optimized to cover as much of the expected Čerenkov ring as possible for given running conditions. Bundles were sometimes placed outside the expected Čerenkov ring region for background studies. Figure 6 shows two typical bundle configurations.

3 Test Conditions

Prototype II was installed in the T9 zone of the CERN PS East Hall. Figure 7 presents a schematic view of the beam line and the experimental setup.

3.1 Prototype II Support Carriage

Prototype II was installed on a carriage which could translate and rotate in several dimensions. The carriage rolled on rails perpendicular to the beam line, changing the distance the Čerenkov light had to travel along the bar to reach the Standoff Box. Prototype II could also be translated vertically to center the beam in the bar, and to vertically scan the bar. The beam entry point at the quartz bar was verified by optical survey. The carriage also allowed Prototype II to rotate on its vertical axis, providing selectable particle incident angles with a precision of about half a degree.

An additional apparatus was used to tilt Prototype II around the bar axis by up to ± 10 degrees. Tilting about the bar axis gave a non-zero azimuthal component to the particle-bar incident angle. Azimuthal tilting was only used to study bar cross-talk, as presented in section 6.8. For all other results, the tilt angle was set to zero.

3.2 The Beamline System

The T9 beam provided unseparated secondary particles in a momentum range between 0.8 and 10 GeV/c. The beam momentum setting accuracy was about 1% of its value. It was operated with positive particles (mainly protons, pions, and positrons) at low intensity, delivering around 10^4 particles to the test area per spill.

The macroscopic beam time structure consisted of a 0.5 seconds spill every 15 seconds. During some periods, the spill period was reduced to 7.5 seconds. Probable micro-structure in the beam spill was not documented, and was never directly observed in these tests.

The beam line was equipped with two gas threshold Čerenkov counters. The counters were pressurized to 3.3 bars, and filled with CO_2 or helium. The CO_2 counter at 3.3 bars identified positrons below around 2 GeV/c, and separated pions and positrons from protons above roughly 3 GeV/c. The helium counter separated positrons from protons and pions below about 6 GeV/c.

Additional beamline particle identification was accomplished using a time-of-flight system (TOF), consisting of two beam counters separated by a flight path of 17 m. The timing resolution of this system was measured to be 115 ps (80 ps per counter) which allowed very good pion/proton separation up to momenta of 7 GeV/c, and pion/kaon separation up to momenta of 3.7 GeV/c (see figure 8).

Comparison of the TOF system with the threshold Čerenkov counters in the overlap of their respective ranges (around 5 GeV/c) indicated negligible cross-contamination of pion and proton samples selected with a simple 3 standard deviations consistency/rejection cut. This selection was used to define the identified particle samples referred to later in this paper.

Three multi-wire proportional chambers (MWPC) were installed on the beam line. The first two chambers were located upstream of the bar. They were separated by about two meters, and served to measure the angle and position of particles incident on the quartz bar. The third chamber was located 2.5 m downstream of the bar, and served to measure scattering in the bar. Each chamber had two wire planes with a wire pitch of 1.27 mm, allowing a precise position measurement in both directions perpendicular to the beam.

Tracks were fit from the MWPCs data using a standard least-squares algorithm. The three chambers were precisely aligned with respect to the beam using the data. The position of the beam relative to the the bar was determined both from survey and from the data. The residuals of high-momentum track fits indicate a root mean squared tracking resolution at the quartz bar of better than 0.5 mm in position and 1 mrad in direction.

The trigger was generated as the coincidence of signals from several plastic scintillation counters. The small size (1 cm by 1 cm) of the furthest upstream trigger counter defined a small solid angle acceptance, and insured that trigger particles intersected the bar. This also limited the trigger rate. The beam profile at the bar for triggering particles was measured to be roughly Gaussian, with a width of approximately 1 cm root mean squared in each transverse direction. The angular spread of triggering particles was approximately 1 mrad.

In addition to this coincidence trigger, roughly 10% of all triggers were randomly initiated by a clock both during and between beam spills. These triggers were used to monitor backgrounds.

A beam halo veto counter made of scintillation counters was installed on the beam line close to the beam extraction. A large scintillation counter was also fixed on the Standoff Box to flag particles crossing the water tank. Another set of counters was arranged along the quartz bar outside the region populated by trigger particles. These counters were used offline to tag events with associated beam halo particles.

3.3 Data Acquisition and Electronics

The Data Acquisition (DAQ) system for Prototype II used VME and CAMAC front-end readout electronics controlled by a UNIX workstation. The connection between UNIX, VME, and CAMAC was made via VIC bus [17]. The control software for the DAQ was written in a combination of C and Tcl/Tk [18]. Stand-alone programs for calibration and online monitoring were written in a combination of C and Fortran 77.

3.3.1 Readout Electronics

The DAQ electronics was housed in four CAMAC crates. One held the main DIRC readout electronics, consisting of a 528 channel LeCroy 2280/2282 10-bit charge integrating (1 count = 0.25 pC) ADC system. Another held pattern units for reading the MWPCs, as well as ADCs and TDCs used to read out the trigger, TOF and veto counters. Two additional crates held 36 LeCroy 4401 modules, which make simultaneous time and pulseheight measurement for PMTs. These 4-channel CAMAC units had a 100 ps intrinsic time resolution with a useful range of 60 ns. The amplitude of signals above the 30 mV discriminator threshold were integrated and digitized with a 1 pC per bit sensitivity. At most 144 PMTs could be read out with this system, but the specific subset of tubes being read out could be quickly changed.

The overall DAQ rate was limited by the average 2280/2282 digitization time of 2.5 ms per event. Digital zero suppression in the 2280 system (with a threshold of 5 counts) gave a low average event channel occupancy, so that data collection did not contribute appreciably to the dead-time.

The Run Control user interface was written in Tcl/Tk. The finite state machine which controlled the DAQ was written in Tcl. The event readout loop was written in two parts: a fast inner loop written in C, and a slower (outer) loop written in Tcl. The fast loop polled for triggers and, upon receiving one, read out the electronics and logged the data to a disk on the SUN station. This double-loop structure allowed efficient data taking together with good user control and monitoring.

Standard calibrations to measure pedestals and gains of the different electronics were performed regularly. In addition, calibrations using an LED flasher and a xenon flasher were used periodically to measure the PMT response.

Twelve high current (up to 50 mA per channel) high voltage power supplies were used to power the PMT bundles. A single power supply fed one or two bundles via a H.V. distribution box. The bundle voltages ranged from 1350 V to 1650 V, and were adjusted to set all the PMT gains within 10% of 1×10^8. The voltages were monitored and adjusted a few times each day, and were found not to drift significantly.

4 Data Sample

Prototype II data were recorded during six run periods of roughly two weeks each, starting in June 1995 and ending in June 1996. Preliminary analysis of the data from the first two periods revealed that the quartz bar surfaces were unacceptably dirty. This was evident from a much larger light loss per internal reflection than expected. The bar was carefully cleaned before the final four data taking periods, and all results presented in this paper come from those data.

The coordinates used to describe the data sample conditions are defined graphically in figure 7. We defined a coordinate system with the z axis as the bar axis, and the y axis across the thickness of the bar in the same general direction as the beam. The x direction was implicitly defined by the right hand rule. The origin of this system was at the Standoff Box end of the bar, where the bar axis intersected the plane of the entrance window. The beam direction was defined by two angles, $\theta_d = -\tan^{-1} b_z/b_y$, and $\varphi = \tan^{-1} b_x/b_y$, where b_x, b_y and b_z are the direction cosines of the beam in the above coordinate system. We defined the effective bar distance Z as the distance traveled by the Čerenkov photons projected along the bar axis. In practice, $Z = z$ when θ_d was positive, and $Z = 2L - z$ when θ_d was negative, where L is the total length of the bar. Data sets were specified by the x and Z position of the intersection of the beam with the surface of the bar, as well as by θ_d and φ.

The data sample can be grouped into five categories, according to the run setup and use in analysis. The data in these groups were taken at different times.

- Z Scan Data

  These data were taken at constant momentum (5.4 GeV) and particle incident angles ($\theta_d = \pm 20°$, $\varphi = 0°$), at varying effective distance Z along the bar. A coarse scan with Z steps of 20 cm was performed over the full Z range (20 cm $\rightarrow$ 460 cm). These data were used to measure the photon yield of Prototype II, as well as the Čerenkov angle resolution. They were also used for systematic studies, and to evaluate the particle identification power of Prototype II. They constitute the largest data sample obtained with Prototype II, comprising several million recorded triggers. In addition to the coarse Z scan, a fine scan with a Z step of 2 cm was performed, covering about 10 cm in range at various Z values. These were special purpose runs with an unusual Standoff Box mirror configuration, as described in section 6.4.

- Momentum Scan Data

These data were taken at constant Z and incident angles, at different beam momenta ranging from 0.8 to 10.5 GeV. These data were used to measure the refractive index of the quartz bar, and to establish the particle identification power of Prototype II as a function of momentum.

- φ Scan Data

  These data were taken when Prototype II was configured with two adjacent short bars, instead of the single long bar used in all other tests. These data were used to check for light cross-talk between adjacent bars.

- Background Tests

  Special studies were performed to understand better the sources of background observed with Prototype II. These included scanning the beam across the bar in the x direction, moving PMT bundles far from the expected Čerenkov rings, and taking data with no water in the Standoff Box.

- Configuration Tests

  Various Prototype II configurations were evaluated with data, to determine which were best. These included a scan of the Standoff Box mirror pitch angle, tests of different PMTs and PMT mounting schemes, and tests of light concentrators on the ends of the PMTs. The results of these tests were used to improve the design of the *BaBar* DIRC.

5 Configuration Tests

To test the PMT immersion in water proposed for the *BaBar* DIRC, 48 PMTs were installed directly in the Standoff Box water. These were installed in two bundles of 24, each arranged in a hexagonal pattern in an aluminium plate replacing one of the nine quartz windows. The tubes were fully immersed, and a long plastic [19] feed-through was glued to the ends of the PMTs to connect them to the outside. The water seal between the feed-through and the plate was achieved with two O-rings. Thirteen 6.5 cm long 1 mm diameter pins were soldered to the normal PMT pins to carry signals and voltages through the feed-through to a custom made base. The base ground was transmitted to the plate via a spring loaded connector. Over a two week test period no water leaks were observed, and the electronics behavior of the PMTs was found to be the same as for tubes in air.

The *BaBar* DIRC proposal to equip each PMT with light concentrators was also tested. In these tests, one of the two 24-PMT bundles described above was equipped with a set of reflective cones. Each cone was 8 mm tall with an outer diameter of 31 mm equal to the PMT spacing, and an inner diameter of 25 mm equal to the photocathode diameter. To facilitate their mounting, ten cones were manufactured together in a single plaque of molded plastic. The cone plaques were polished and coated with a 600 nm Al layer followed by 200 nm of SiO_2. The light collection improvement using the concentrators measured in the Prototype II test was consistent with lab measurements, though their reflectivity was found to decrease by about 10% during their two week exposure to water. Research to improve the long-term reflectivity is in progress.

6 Data Analysis and Results

In this section the Prototype II data analysis methods and results are presented. First the general methods used in all analyses are described, then the specific analyses of the performance of Prototype II as a particle identification device. The topics described here were selected to highlight this performance, and are representative of all the tests which have been performed, but are not an exhaustive set.

Analysis results involve the reconstruction of Čerenkov photon production information from observed PMT signals. The conventions to describe this reconstruction build on those defined in section 4. We use the symbol θ_c to define the production cone opening angle in quartz, and ϕ_c to define the azimuthal angle of Čerenkov photon production. For runs at $\varphi = 0$, photons emitted in the y-z plane toward the Standoff Box are defined as $\phi_c = 0$. With this convention, the Prototype II acceptance covered a symmetric fraction of the Čerenkov cone around $\phi_c = 0$ for positive θ_d, and around $\phi_c = \pi$ for negative θ_d.

The angle θ_y was defined as the angle with respect to the y-axis of the photon momentum projected in the y-z plane, that is to say $\theta_y = -\tan^{-1}(c_z/c_y)$, where c_x, c_y and c_z are the direction cosines of the photon at emission. By convention, θ_y is positive when the photon travels toward the Standoff Box. In general, θ_y is a function of θ_d, θ_c and ϕ_c ($\sin\theta_y = \sin\theta_d \cos\theta_c + \cos\theta_d \sin\theta_c \cos\phi_c$), and is simply equal to $\theta_d + \theta_c$ when $\phi_c = 0$.

6.1 Run and Event Selection

Good runs for analysis were selected based on the observed beam conditions (background rates and trigger rates) and on the observed detector performance for simple measurements (single-photon spectra and calibration results). Events for analysis were selected from beam-triggered data based on cuts designed to reduce backgrounds. Table 1 gives an example of the effect of the selection cuts on a typical run at 5.4 GeV/c.

The first selection cut was to verify the trigger condition using the offline readout information. Events with hits in halo counters were rejected. Exactly one reconstructed track was required for each trigger. The reconstructed track position at the bar was required to lie within a chosen fiducial area (generally well within the bar). Events with extra MWPC hits (not used in reconstructing the single track) were rejected. Events with a large number of PMT hits (more than four standard deviations beyond the number expected for Čerenkov light from a single particle) were also rejected. The additional hits in these events are believed to come from Čerenkov light generated by halo particles traversing the water in the Standoff Box. This interpretation is consistent with the observed spatial distribution of the hits, their pulse height distribution, and the dependence of the occurrence of such events on beam conditions (see section 6.10.1). An unambiguous PID in at least one of the beam line systems was required, and the two were required to agree on the PID when the particle momentum allowed both to be used.

6.2 Hit Selection and Correction

For each run, noisy electronics channels were identified using random-triggered data, and were removed from analyses of that run. In analyses requiring a consistent data set, the logical OR of the noisy channels over the set were removed. Electronics gains were computed in dedicated calibration runs immediately preceding the data runs, and were used to correct for channel-to-channel variations. PMT gains were measured for each run from the data, by fitting the single photon spectrum for each tube bundle. After correcting for the net gain, a common threshold set above the online sparsification cut was applied to all channels, to insure uniform electronic acceptance.

A *hit* was defined as a channel whose corrected signal was above this threshold. The random background hit rate (from electronics noise, dark current, and cosmic rays) was measured using randomly triggered data (see section 6.10.1). This noise hit rate was subtracted statistically from the data channel by channel during analysis.

Using the reconstructed track, both θ_c and ϕ_c were calculated for each hit, assuming it was generated by a Čerenkov photon from that track, modulo discrete ambiguities. In the absence of further information, the ambiguity was 'resolved' by random assignment among the possible interpretations. The θ_c values for the ambiguous solutions were generally degenerate.

For a given geometric configuration (tube position and bar-beam configuration), the Čerenkov solid angle subtended by the active area of a tube was calculated a-priori, exploiting the fact that the beam angular divergence was very small. This calculated solid angle was used to correct the hit rates for geometric acceptance in analysis.

The LED calibration system was not sufficiently uniform to allow a measurement of the relative PMT quantum efficiencies. To account for tube-to-tube quantum efficiency variation, a relative 16% error was added in quadrature to the hit rate statistical errors. This additional 16% error made the χ^2 per degree of freedom average to about one for the fits to signal plus background for the runs at $\theta_d = -20°$. In many cases, this was the dominant error on the hit rate. While this formula treats a systematic effect statistically, it was found generally to give reasonable results as measured by fit quality parameters. In some cases a more sophisticated treatment of the quantum efficiency uncertainty was used, as in section 6.5.

6.3 Čerenkov Angle Resolution per Photon

The single photon θ_c resolution of Prototype II is demonstrated in figure 9. This shows the distribution of corrected average hit rate versus reconstructed θ_c for a subset of PMTs for pion data at $\theta_d = -20^\circ$ and $Z = 220\,\mathrm{cm}$. The data plotted were restricted to the range $|\phi_c| < 0.3\,\mathrm{rad}$, where the tubes had a good solid angle acceptance and hence high statistics. A Čerenkov signal is clearly visible, with a central value consistent with expectations. Residual background is also visible as a non-zero hit rate far from the Čerenkov peak. The composition of this residual background is discussed in section 6.10.

The data fit well to a Gaussian for the Čerenkov signal plus a flat distribution for the background. The θ_c resolution was defined as the Gaussian σ parameter of this fit. The single photon θ_c resolution for pions was found to be $10.0 \pm 0.2\,\mathrm{mrad}$, in agreement with Monte Carlo expectations. Similar analysis of protons and electrons gave consistent results. No significant variation in this resolution with either Z (photon transmission distance down the bar) or ϕ_c (photon position within the Čerenkov ring) was observed, within the calculated errors of the data. The ability to measure the single photon θ_c resolution was diminished by the effect described in section 6.4 at small Z, and by poor statistics at large $|\phi_c|$.

6.4 Fine Z Scan Analysis

Figure 10 plots the corrected hit rate as a function of Z for a single tube over the fine Z scan data sample. These data were taken under altered conditions in that the Standoff Box mirror was disabled. The absence of a Standoff Box mirror means that any photon leaving the bar end headed towards the mirror was lost, while those headed towards the PMTs were detected normally. The data show an oscillation of the hit rate with Z, whose amplitude decays approximately exponentially. This effect can be understood by a simple model of the DIRC.

The oscillations occur because the Čerenkov photons travel the bar along a nearly predictable path. The photons exit the bar bouncing either towards or away from the Standoff Box mirror, depending on their ϕ_c and Z. The fraction of photons leaving the bar pointed towards the mirror is expected to oscillate as a function of Z with a period of $2t\tan\theta_y$, t being the thickness of the bar. This behavior is confirmed by the data shown in figure 10.

The oscillation decay demonstrates that the photon propagation is not fully predictable. The natural dispersion in the Čerenkov production angle gradually mixes the photon paths. By the time the photons have propagated a few meters, this dispersion randomizes the phase of individual photon paths, washing out the oscillations. The damping rate of these oscillations is well reproduced by the Monte Carlo simulation. It should be noted that in the *BABAR* DIRC, the minimum photon transmission distance will be nearly two meters, and the average much more.

The oscillation effect is greatly reduced when the Standoff Box mirror is in place, as the mirror recovers most of the photons lost in figure 10. A residue however persists because of the imperfect mirror efficiency, and because the reflected image does not lie exactly on top of the direct image. This residual oscillation effect is sufficiently powerful to noticeably distort the effective hit rate at small Z. The introduction in the new *BABAR* DIRC design of a quartz wedge at the end of each bar will reduce these residual effects, since its reflectivity is nearly unity, and because it places the reflected image more nearly on top of the direct image.

6.5 Photoelectron Yield and Attenuation

The photoelectron yield of Prototype II was measured with the coarse Z scan data. Another result of this analysis was the attenuation rate for Čerenkov photons as they traveled down the bar. This analysis proceeded in two steps. First, the photoelectron rate per-track at a given Z value was determined. This was defined as the area of the Gaussian in a Gaussian plus a flat background fit to the θ_c distribution of the hit rates (as in figure 9). The photoelectron rate was measured in the central region of Prototype II (approximately $|\phi_c| < 0.6\,\mathrm{rad}$), where the acceptance corrections were small and well understood. Pion and proton fits were performed separately and then averaged. The photoelectron rate as a function of Z was then fit to a modified exponential. The Prototype II photoelectron yield was defined as the extrapolation of this fit to zero transmission length, and the attenuation as the decay parameter in the exponential.

In this analysis, a more sophisticated technique was needed to treat the unknown PMT quantum efficiencies. Because the same PMTs were illuminated at every Z, the quantum efficiency uncertainties were fully correlated between measurements, and could not be treated statistically. Instead, the data itself was used to estimate the efficiencies and remove this uncertainty from the data.

To do this, a single efficiency correction factor per tube was introduced simultaneously to the fits of pion and proton samples for most of the Z scan data sample. Runs where residual oscillation effects (see section 6.4) were believed to be large were not included in the tube efficiency determination. The use of 11 runs gave 22 independent constraints on each tube efficiency. The hit rate weighted average correction was constrained to unity.

The corrected tube hit rates for the full Z scan data were adjusted for this efficiency before fitting for the photoelectron rate. The statistical error on the efficiency fit was added in quadrature to the photoelectron rate errors, before fitting for the photoelectron yield, as a coherent effect across Z. An error was also added for the estimated 0.9 mrad uncertainty in the θ_c position of the PMTs on the image plane. This error was propagated to the hit rates, as was the efficiency factor error.

For data at small Z, the oscillation effect described in section 6.4 also affected the hit rates. This was accommodated by adding to the photoelectron rate errors an estimate of the effective error induced by the residual oscillation effect. This error was estimated from the data as the root mean squared of the difference in the hit rates for small changes in Z. These errors dominate the hit rate errors for $Z < 1$ meter, but are negligible for $Z > 2.4$ meters.

The area of the Gaussian at each Z value was converted into a measure of the Čerenkov quality factor N_0. This is defined by the relation $\epsilon_{geom} \times N_0 \times \sin^2\theta_c =$ the number of photoelectrons detected per centimeter of radiator over the acceptance of Prototype II. This definition of N_0 differs slightly from the one conventionally used with threshold Čerenkov detectors [20] in that the geometric acceptance ϵ_{geom}, which accounts for the truncation of the Čerenkov cone and for the partial coverage of the image plane by PMTs, has been explicitly extracted. In this definition, N_0 is proportional to the product of the photodetection efficiency and the collection efficiency ϵ_{coll}, which accounts for the light losses during photon transmission and reflection. A numerical estimate for ϵ_{coll} is given in section 6.5.1. For the DIRC N_0 is a function of Z.

Figure 11 shows the measurements of $N_0(Z)$ versus Z. The data are fit to an exponential with a discontinuity at $Z = 240$ cm, to account for reflection loss at the bar-end mirror. The fit gives a χ^2 of 24 for 18 degrees of freedom, and the fitted values for the three parameters are

$$\begin{array}{rcrcl} N_0(0) & = & 106.9 & \pm & 1.3 \text{ cm}^{-1} \\ \text{attenuation per meter} & = & 4.1 & \pm & 0.7\ \% \\ \text{loss at the mirror} & = & 11.4 & \pm & 1.5\ \% \end{array}$$

The errors quoted above are those returned from the fit, and so include the full statistical and systematic error on the photon rates, but not any systematic error due to the fit model itself. In this fit the potential loss of light at the glue joint at $Z = 120$ cm (and $Z = 360$ cm) is ignored. Fits with this loss as a free parameter were also performed. The glue joint light loss could not be measured precisely and was found to be consistent with zero within two standard deviations. Lab measurements and other tests also indicate a negligible light loss at the glue joint. Neglecting the glue joint loss leads to a conservative (larger) estimate of the attenuation, and has no effect on the estimate of $N_0(0)$. In the final *BABAR* DIRC the same configuration (namely a 1.2 m long quartz bar followed by a glue joint) will be repeated four times. The result of the fit performed without explicit inclusion of the glue joint thus defines an effective attenuation in quartz relevant for the *BABAR* DIRC.

This measurement of the attenuation value agrees well with a full Monte Carlo simulation, which includes the spectral response of the PMTs, the spectral transmission of bulk natural quartz, and an internal reflection coefficient of 0.9995 [10]. This last is somewhat smaller than recent direct measurements performed on bars made of synthetic quartz (synthetic quartz will be used in the *BABAR* DIRC for radiation hardness reasons [21]). This measured attenuation value is better (smaller) than the one used to estimate the physics performance of the *BABAR* DIRC in the *BABAR* TDR [2].

Systematic errors on these results were estimated by varying the analysis cuts. Changing the hit selection threshold by a factor of two had a negligible effect on the results. Changing the ϕ_c range of tubes used for the fit also had no appreciable effect. In these and other checks, additional systematic errors were found to be negligible compared to the fit errors, which contain the systematic errors on quantum efficiency uncertainty, position uncertainty, and the oscillation effect.

6.5.1 Collection Efficiency and N_0 Estimate

To facilitate comparing this $N_0(0)$ measurement with other N_0 measurements, the effects peculiar to the Prototype II test setup implicit in ϵ_{coll} must be divided out. There is no way to measure ϵ_{coll} directly from the data. However, a realistic estimate of ϵ_{coll} at $Z = 0$ can be calculated by combining expected light-loss effects from the different parts of Prototype II. Simple optical calculations show that about 2% of the photons are lost at the interface of each of the two quartz windows. Lab tests have shown the reflectivity of the Standoff Box mirror was 88% prior to installation in the wavelength range relevant for Prototype II, and $80.6 \pm 0.5\%$ after two months in the water. Since on average 50% of the light is direct, and assuming a 84% reflectivity, this contributes 8% to the net photon loss. Light absorption in the Standoff Box water was estimated as 10% per meter over an average distance of 1.2 m. The threshold cut for defining a hit was analyzed using the data and found to remove 7% of the real photons.

Combining these losses gives the estimate $\epsilon_{coll} \simeq 73\%$ at $Z = 0$, which leads to:

$$N_0(0)/\epsilon_{coll} = 146 \pm 1.8 \pm 9\,\mathrm{cm}^{-1}$$

The first error comes from the N_0 fit error, the second from an estimated 30% uncertainty in the light loss estimates. This value is in agreement with the value of $137\,\mathrm{cm}^{-1}$ that was used for performance estimates of the *BaBar* DIRC in the *BaBar* TDR [2].

6.6 Čerenkov Angle Resolution per Track

To measure θ_c for a single particle (track), the individual θ_c measurements from the different hits in a single event must be combined. Because of the backgrounds and non-uniform acceptance in Prototype II, this combination was best performed using a maximum likelihood fit. The parent function used to describe the data in θ_c was a Gaussian signal plus a flat background. The width of the Gaussian was fixed to the 10.0 mrad value measured with single hits (see 6.3). The amplitude of the signal was set according to the tube acceptance (as a function of ϕ_c), while the background amplitude was assumed to be independent of ϕ_c. The free parameters of the fit were the position of the Čerenkov ring and the total number of background photoelectrons. The number of signal photoelectrons was trivially extracted by subtracting the number of background photoelectrons from the total. The fit included all hits within the range $|\phi_c| < 1.0$ rad and $760\,\mathrm{mrad} < \theta_c < 980\,\mathrm{mrad}$, about 85% of the Prototype II PMTs.

The ring fit analysis was performed on the same data sample used to measure the photoelectron yield and attenuation, namely the $\theta_d = \pm 20°$ $5.4\,\mathrm{GeV}/c$ coarse Z scan data. This provided several results, as summarized below:

- The distribution of the fitted number of signal photoelectrons was observed to agree well with the expected Poisson distribution. For the run at $Z = 260$ cm the average number of signal photoelectrons was measured to be 10. Given the greater tube density and larger coverage, this corresponds to an expected average of 20 signal photoelectrons in the *BaBar* DIRC for similar tracks (in the *BaBar* DIRC, a track dip angle of 20° is very near the minimum for the number of detected photoelectrons. Some other angles give over twice as many accepted photoelectrons).

- The number of signal photoelectrons as a function of Z was used to extract a value for the attenuation and mirror loss independent of the method described in section 6.5. The results were consistent within 1 standard deviation for both quantities. These fits were used to establish the scale of the number of photoelectrons that is shown on the right hand side of figure 11.

- The track θ_c resolution was fit to a standard form as a function of the observed number of signal photoelectrons N_γ. The resolution was measured as the standard deviation of the track fit θ_c values, according to the number of signal photoelectrons N_γ. The fit function parameterized the track θ_c resolution as:

$$\sigma_R{}^2 = \left(\frac{f \times \sigma_S}{N_\gamma}\right)^2 + \sigma_0{}^2$$

The free parameters in the fit were σ_S and σ_0. σ_S can be interpreted as the effective single photon θ_c resolution, while σ_0 modeled coherent resolution effects, such as the track angular resolution, or tube mis-alignments. The quantity f modeled the expected resolution deterioration due to the background, as calculated using Monte Carlo. For the measured background rate, f was determined to range from 1.12 at $N_\gamma = 15$ to 1.25 for $N_\gamma = 5$. The extracted value $\sigma_S = 9.9 \pm 0.3\,\mathrm{mrad}$ is consistent with the single photon θ_c resolution quoted in section 6.3. The extracted value $\sigma_0 = 1.1 \pm 0.3\,\mathrm{mrad}$ is consistent with estimates of tracking errors and tube mis-alignments.

6.7 Prototype II Particle Identification

The particle identification power of Prototype II was measured for pions and protons at 5.4 GeV/c. At this momentum, the θ_c separation between pion and proton Čerenkov rings has the same value as between pions and kaons at 3 GeV/c. The momentum 3 GeV/c corresponds roughly to that of decay products from a two-body B^0 decay in *BABAR* hitting the DIRC bar at the same 20° value of θ_d. In this decay mode, pion/kaon separation is essential for the physics goal of the *BABAR* experiment. Thus the pion/proton separation at 5.4 GeV/c tests the performance of Prototype II in a situation relevant for the *BABAR* DIRC.

The particle separation power was defined as the difference in the θ_c peak position values for the track fits described above, divided by the root mean squared of the pion track θ_c distribution. This is shown in figure 12. The pion track θ_c root mean squared was measured for data at $Z = 220$ cm (to be far from the coherent effect region), and found to be 3.6 mrad. The peak separation was measured in the same data to be 13 mrad, consistent with expectations. These together give a pion/proton PID power for Prototype II of 3.6 standard deviations.

The PID power of Prototype II was also studied using the momentum scan data taken at $\theta_d = 20°$. The limited θ_c coverage of Prototype II restricted the usable momentum range to above 3 GeV/c. The results of this study are shown in figure 13. This plots the track θ_c value for pions and protons averaged over a full run. The data were fit to the known θ_c momentum dependence, with the quartz index of refraction n_q as a free parameter. The fit gave $n_q = 1.474 \pm 0.001$ (statistical error only), in good agreement with a detailed Monte Carlo study.

6.8 Adjacent Bar Cross-Talk

To test for possible light cross-talk between adjacent bars, Prototype II was re-fitted with a bar box containing two short (1.2 meter long) adjacent and parallel bars. The bars were separated in the x direction by a $75\,\mu$m air gap along their full length. For these tests Prototype II was rotated 10 degrees around the bar axis, which insured that the photon paths included bounces off the nearest-neighbor bar surfaces. In this configuration, photons bouncing down one bar could conceivably 'escape' and re-enter the other bar, generating light cross-talk. The PMT layout for these runs at $\varphi = 10°$ is shown on the right side of figure 6.

Runs were taken in this configuration for various beam x (transverse) positions across the bars. Simple photoelectron counting as a function of x was used to locate the x position of the bar gap (the variation in photoelectron rate across a bar edge will be a powerful method for aligning the *BaBar* DIRC from data). Once the gap was located, the beam was directed into the center of one or the other bar, far from the gap.

Data taken in the bar centers were used to establish the position of the Čerenkov images generated by each bar. The distribution of hits in the image plane was fit to the usual single Gaussian signal plus a flat background. As expected, the image positions from the different bars were found to be separated by an amount equal to the separation between the bar centers (4 cm). This separation was best detectable in the branches of the Čerenkov image at large $|\phi_c|$, where the image cuts across the x direction. Only tubes at large $|\phi_c|$ were used for the cross-talk measurement.

Once the positions of the different images were established, a new fit was performed allowing for the presence of a second cross-talk peak at the position of the other bar's signal. The fit value for the amplitude of this second peak was found to be consistent with zero, providing no evidence for light cross-talk. Taking only the statistical errors on the fit, a 95% confidence level upper limit on the light cross-talk was set at 3.0%.

6.9 Timing Resolution

Some of the Prototype II PMT bundles were equipped with combined TDC/ADC readout electronics [22], as described in section 3.3.1. In the *BaBar* DIRC, all the PMTs will be equipped with TDCs. The timing information they provide will be used to reduce backgrounds, in particular arising from other tracks in an event. Simulation studies have shown that this background rejection is important for ring pattern recognition. The effectiveness of this background rejection depends on the timing resolution. This was measured in Prototype II using the timing information. Prototype II timing information was also used to analyze the different sources of background, as presented in section 6.10.

The timing resolution was studied in Prototype II in data taken at $\theta_d = 0°$. In this configuration the Čerenkov light is split into two parts, one proceeding directly to the image plane, the other first bouncing off the mirror at the far end of the bar. These two images are spatially degenerate, but well separated in time due to the different path lengths.

An example of these data are shown in figure 14. This plots the arrival time for hits in TDC-equipped PMTs. The plot clearly exhibits the two peaks expected for the Čerenkov signal, one each for direct and bar-end mirror reflected photons. The late arriving peak is associated with the reflected signal, and is smaller than the direct signal peak due to photon attenuation during bar transmission and reflection loss at the end-mirror.

The data in figure 14 were corrected for several effects. The relative time offset of the different PMTs coming from the combined effects of PMT transit time, electronic signal effects, and light propagation in the bar, have been subtracted. These offsets were measured from the data for each channel by comparing the time peak positions for data at different Z values. The TDC information was corrected for several small electronics problems, including a small correlation between the ADC and TDC values (due to slewing). The absolute time/count relation was determined offline.

The timing resolution was extracted from a fit to the data, as shown in figure 14. The fit included two Gaussian signal peaks plus a polynomial background. The timing resolution is the same for the direct and the reflected light and was measured to be $2.4 \pm 0.1 \pm 0.3$ ns (statistical and systematic errors). The systematic error comes from an asymmetry in the TDC signal spectra, which is due to charge-time correlations and transit time differences for different hit locations on the photo-cathode. The measured resolution is consistent with the transit time fluctuations expected for these PMTs (2 ns). The *BaBar* DIRC will use PMTs with a 1.8 ns transit time spread [7].

6.10 Prototype II Backgrounds

As was noted in figure 9, residual background is present in the Prototype II data even after random effects are subtracted. The remaining background rate is small relative to the signal ($12.0 \pm 0.5 \times 10^{-3}$ hits per tube and per event, about 5% of the signal at the peak). By comparison, the intrinsic 'background' from the crossing rings created by real tracks in $B\overline{B}$ events at *BaBar* (on average six tracks per event) is expected to be a few percent of the peak signal.

To understand the origin of this background, special studies were performed. These attempted to distinguish backgrounds which were unique to Prototype II and its test environment from those intrinsic to the DIRC concept, in order to predict the background rate for the *BaBar* DIRC. These studies were performed on different data samples, not all taken under identical Prototype II configurations and beam conditions. A number of potential background sources are discussed in the following sections.

6.10.1 Random Backgrounds and Beam-Related Backgrounds

Purely random backgrounds (thermal electrons in the PMTs, electronic noise, cosmic rays, radioactivity, light leaks, and time independent beam-related backgrounds) were treated statistically using the random-triggered data as described in the analyses presented above. The random background rate is purely a function of the detector equipment and environment, and so can be estimated directly for the *BaBar* DIRC without the use of the test beam data. Thus the specific makeup and sources of the Prototype II random background were not investigated.

Due to the pulsed nature of the beam, a random trigger was not adequate to eliminate fully the beam-related backgrounds. The beam halo created backgrounds in Prototype II either by striking the Standoff Box and generating Čerenkov photons in the water, or by striking the quartz bar and generating an additional Čerenkov image. The former background was studied in part using the correlations with the veto counters located against the Standoff Box. The observed high multiplicity of hits for these events (69 ± 2 hits per event in average) was well reproduced by the Monte Carlo simulation. The occurrence of such events as a function of the beam position with respect to the Standoff Box matched expectations. This background was removed by a set of cuts on total multiplicity and bundle occupancies. It will be present at some level in the *BABAR* DIRC, with a muon halo accompanying the beams, but the rate should be modest (of order 1 kHz), and its nuisance reduced by the fact that the *BABAR* Standoff Box will have fewer reflecting surfaces.

The remaining beam-related background was shown to be independent of whether the triggering track hit the bar or not. Special runs, where the beam was not centered on the bar, were used to estimate this background. The corrected hit rates measured in such a special run are shown in figure 15. The left side plot shows the hit rate for events in which the track hit the bar, fit to a Gaussian signal plus flat background. The right side shows the same data where the hit rate for events in which the track did not hit the bar has been subtracted, removing the correlated beam background. The data are consistent with a fit to a flat background, but the statistics are insufficient to rule out other possible background distributions (such as a wider Gaussian). The Prototype II beam background is clearly specific to that device and those tests, and cannot be extrapolated to the *BABAR* DIRC. There is a small residual background, however, that seems intrinsic to the DIRC concept, and will be present at some level in the *BABAR* data. This background is discussed in more detail in the next section.

6.10.2 Track-Related Backgrounds

Figure 15 demonstrates that a small amount of background in the Prototype II data ($3.5 \pm 0.7 \times 10^{-3}$ hits per tube and per event, about 1.5% of the signal at the peak) does not come from random or beam related effects, but is instead associated with the track itself. This can also be demonstrated by looking at the time distributions for a PMT bundle far away from the Čerenkov ring, as shown on figure 16. On the left part of the plot, the triggering particle does not cross the bar, and the time distribution due to random and beam-related background is flat. The right part of the plot shows the time distribution for the same bundle when the particle crosses the bar. A relationship with the track crossing the bar is demonstrated from the narrow in-time peak in the background time spectrum (the constant background level also slightly increased). The hypothesis of an electronic crosstalk origin for this peak was ruled out.

This track-related component of the background was studied. The two main features of this background are that its level is flat in θ_c, even far from the signal, and that it stays in-time with Čerenkov photons independent of the considered PMT position. The latter feature indicates that the background photons propagate in the bar with angles similar to those of Čerenkov photons.

Possible physical origins for the track-related background are as follows :

- Reflected Čerenkov light

  While the Prototype II image plane only accepted 60° of the Čerenkov image, the rest of the image at large ϕ_c values still entered the Standoff Box. Because the Standoff Box interior was reflective (unpainted aluminum), the remaining photons could have reflected to the image plane and generated background hits. Even though the aluminum surface of the Standoff Box was rough, it is difficult to explain how the reflected Čerenkov photons could generate the observed homogeneous spatial distribution. The reflected Čerenkov light background does not translate to the *BaBar* DIRC, as that will have a non-reflecting inner surface.

- Delta-ray Čerenkov light

  The delta-rays generated by the track passing through the bar can themselves generate Čerenkov photons. Simple calculations of this effect give a background rate of 5% relative to the main signal, with a wide spatial distribution. Even though they are correlated with the track, these photons would not produce the observed background in-time peak over the full image plane. They may however contribute to the observed increase in the overall (time uncorrelated) background rate associated with a track in the bar. Delta-ray background will also be present in the *BaBar* DIRC.

- Non-Čerenkov light

  Čerenkov radiation is not the only effect which generates light when particles pass through matter. In particular, some scintillation light is expected. Direct measurements of this effect in a dedicated test beam showed it to be very small [23]. Furthermore, the propagation time distribution of scintillation photons would be different from that observed for track-related background. Scintillation light background is not expected to contribute in any noticeable way to the *BaBar* DIRC background.

- Scattered Čerenkov light

  The transmission coefficients of the bar, water, mirrors, and interfaces of Prototype II were not unity. If the light lost to the Čerenkov image during transmission were scattered instead of absorbed, it could reappear as background. However, the track-related background rate was observed not to depend on Z, and its timing distribution showed the same Z dependence as the signal. Consequently, scattering in the bar was ruled out as the dominant source of track-related background. While scattering after the photons exited the bar would produce the observed in-time peak of the track-related background, it was not possible to identify an obvious source of scattering through visual inspection of the windows and mirrors. Furthermore, dedicated runs with the water drained from the Standoff Box showed comparable track-related background rates, eliminating the water as a significant scattering source. Scattered Čerenkov light background could also be present in the *BaBar* DIRC, but its magnitude remains uncertain.

These studies were unable to identify a single coherent model of track-related background. The possibility that several different sources might have combined to produce the observed background cannot be excluded. However, the total observed track-related background rate was small. If the *BaBar* DIRC experiences the same rate of track-related background, it will not appreciably impact its expected performance.

7 Conclusions

The DIRC has many attractive features and is well matched to the requirements for a particle identification device in the BaBar detector at the PEP-II B Factory. In particular, the final system is expected to yield excellent π/K separation of nearly four standard deviations or better over the entire acceptance region for all of the products from B decay. An extensive prototype program, progressing through a number of different prototypes [6], demonstrated that the principles of operation were well understood, and provided initial estimates of performance which were incorporated into studies made in the *BaBar* TDR [2].

The beam tests of the large scale Prototype II, described in this paper, have refined these earlier measurements and have confirmed the stable and robust operation of the DIRC concept. A wide variety of studies were performed with this system to address a spectrum of mechanical and system performance issues. These studies include data taken at a variety of different incident angles, track position along the bar, and momenta, with different particle types. The Prototype II mechanical realization, though not completely optimized, performed very well. Operationally, the system was stable, and ran smoothly. High quality data were taken throughout all run periods. No water leaks developed during operations and the water remained transparent over the typical two week run periods without re-circulation. Operation of the photomultiplier tubes in water during the final run periods was also completely satisfactory.

The measured behavior for single photons was consistent with design expectations, and confirmed the experience with earlier prototypes. In particular, the observed single photon resolution was 10.0 ± 0.2 mrad, as expected, and essentially independent of particle type, track position in the bar, or Čerenkov azimuthal angle. The effective total photon attenuation length near the image center, following bar cleaning, was measured to be $4.1 \pm 0.7\,\%$ per meter of bar length at a track angle of 20 degrees, substantially better than seen in earlier prototypes, and consistent with direct optical test bench measurements of the bars. After correcting for geometrical acceptance and estimated collection effects, the number of photoelectrons observed was measured to be $146 \pm 1.8 \pm 9\,\mathrm{cm}^{-1}$, at zero transmission distance. This value is consistent with earlier prototypes results and with the value used in simulations for the TDR performance estimates. Scans across the gap region between bars showed that there is no measurable cross talk between bars mounted in close proximity side-by-side. Finally, the relationship between timing and photon position at the detector was shown to be very useful for background rejection. The single photon timing resolution of 2.4 ns was dominated, as expected, by the transit time spread of the PMTs used in the test.

Track based results combined the single photons together with tracking to produce identification information for each track. The results obtained depended on track momentum and dip angle, the number of photons observed, and other factors, in agreement with simulations. For example, the separation observed between 5.4 GeV/c pions and protons at $\theta_d = 20^\circ$ was 3.6 standard deviations for tracks 220 cm from the Standoff Box. The resolution was observed to scale approximately as the square root of the number of photons, with a small residual term of about 1.1 mrad coming from correlated factors such as track multiple scattering in the bar, and residual alignment uncertainties. The effective index of refraction of the quartz radiator was measured to be $n_q = 1.474$ from a direct fit to the momentum dependent Čerenkov angle.

In conclusion, the tests were very successful and no significant, unanticipated variance in performance as a function of the position or angle of the track in the DIRC bar was observed. All tests planned for this prototype are now complete, and design, engineering, and construction of the *BaBar* DIRC are underway.

We would like to thank the CERN staff for excellent beam delivery, and G. Bertalmio for his assistance and technical support during the beam tests at CERN.

References

[1] *An Asymmetric B Factory Based on PEP: Conceptual Design Report*, LBL-PUB-5303/SLAC-REP-372 (1991)

[2] *The BaBar Collaboration, Technical Design Report*, SLAC-REP-950457 (1995)

[3] See for example:
J.D. Jackson, *Classical Electrodynamics*, 2nd edition (John Wiley & Sons, New York, 1975)
W.W.M Alison and P.R.S. Wright, *The Physics of Charged Particle Identification: dE/dx, Čerenkov Radiation and Transition Radiation*, p. 371 in *Experimental Techniques in High Energy Physics*, T. Ferbel editor (Addison-Wesley, 1987)

[4] See for example:
J. Seguinot and T. Ypsilantis, *Nucl. Instr. Methods* A 343 (1994) 1
T. Ypsilantis and J. Seguinot, *Nucl. Instr. Methods* A 343 (1994) 30
W. Adam *et al.*, *Nucl. Instr. Methods* A 343 (1994) 68
K. Abe *et al.*, *Nucl. Instr. Methods* A 343 (1994) 74

[5] B.N. Ratcliff, SLAC-PUB-5946 (1992) and Dallas HEP (1992) 1889
B.N. Ratcliff, slac-pub-6047 (1993)
P. Coyle *et al.*, *Nucl. Instr. Methods* A 343 (1994) 292

[6] D. Aston *et al.*, *Test of a Conceptual Prototype of the Total Internal Reflection Cherenkov Imaging Detector (DIRC) with Cosmic Muons*, *IEEE Trans. Nucl. Sci.* NS-42 (1995) 534

[7] PMT model 9125, Thorn EMI Electron Tubes, Bury Street, Ruislip, Middlesex HA47TA, U.K.

[8] Quartz Products Co., 1600 W. Lee St., Louisville, Kentucky 40201

[9] Zygo Corporation, Laurel Brook Road, Middlefield, Connecticut 06455

[10] H. Krueger *et al.*, *Initial Measurements of Quartz Transmisson, Internal reflection Coefficient and the Radiation Damage*, *BABAR* DIRC Note #18 (Jan. 96)
H. Krueger *et al.*, *The Optical Scanning System for the Quartz Bar Quality Control*, *BABAR* DIRC Note #54 (Oct. 96)

[11] EPO-TEK 301-2, Epoxy Technology Inc., 14 Fortune Drive, Billbrica, Massachusetts 01821

[12] RTV Q3-6093, Dow Corning

[13] VITON, DuPont Co.

[14] Optical Coating Laboratory Inc. (OCLI) 2789 Northpoint Pkwy, Santa Rosa, California 95407

[15] PMT model R268, Hamamatsu Co., 250 Wood Ave, Middlesex, New Jersey 08846

[16] RTV BC-634K, Bicron, 12345 Kinsman Rd., Newbury, Ohio 44065

[17] Creative Electronics Systems S.A., VIC bus

[18] J. Ousterhout, *Tcl and the Tk Toolkit* (Addison-Wesley 1994)

[19] ULTEM 1000 polyetherimide, General Electric Co.

[20] Particle Data Group, *Review of Particle Properties*, Physical Review **D45**, Part 2 (1992)

[21] X. Sarazin *et al.*, *Radiation Damage of Synthetic Quartz and Optical Glues*, *BABAR* DIRC Note #39 (May 96)

[22] S. Plaszyzynski *et al.*, *The* TDC *system for* DIRC Prototype II, *Hardware Description and Performances*, *BABAR* DIRC Note #10 (Sept. 95)

[23] P. Besson *et al.*, *Propagation of Photons Induced by a Proton Beam in a Quartz Bar*, *BABAR* DIRC Note #3 (Aug. 95)

Triggers	50 000
Offline trigger	45 000
Track Fit	22 000
Extra MWPC Hits	13 500
Large # Hits	8 000
Beam line PID	4 500
Selected pions	3 000
Selected protons	1 500

Table 1: Event selections for a typical run at 5.4 GeV/c.

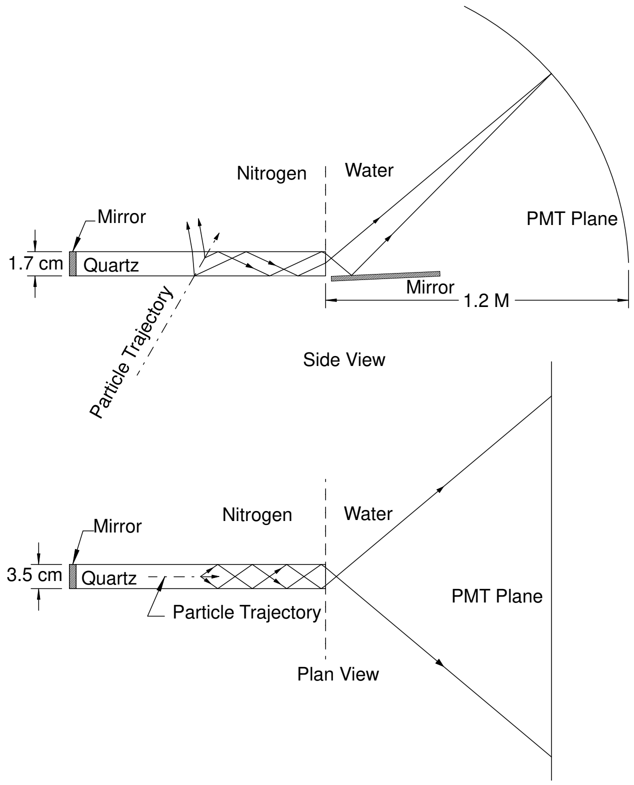

Figure 1: Schematic of a single radiator bar of a DIRC counter. The particle trajectory is shown as a dot-dash line, the Čerenkov photons as solid lines with arrows.

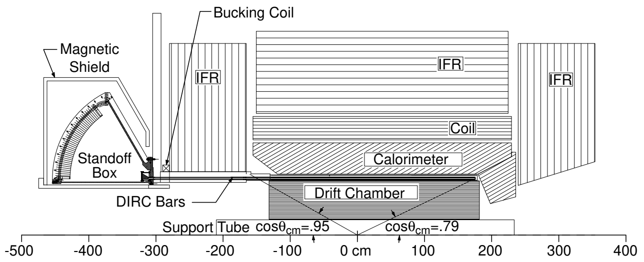

Figure 2: Schematic midplane section of the top half of the *BaBar* detector and its DIRC. The high momentum beam will be incident from the left, defining the forward direction.

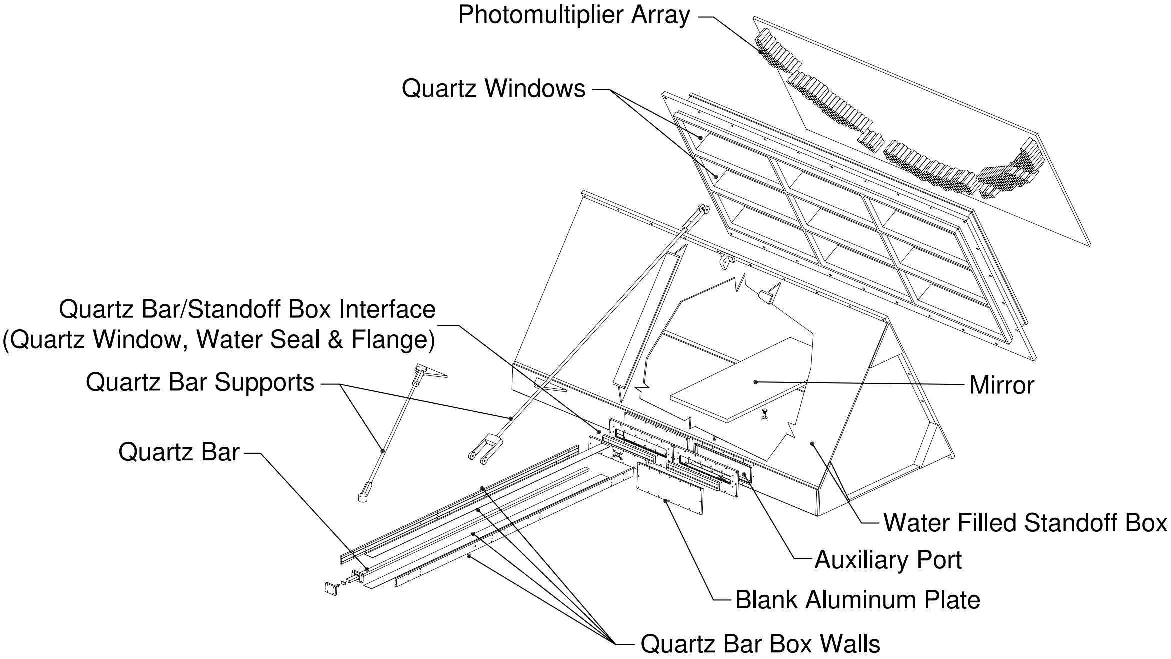

Figure 3: Isometric drawing of Prototype II.

Figure 4: Photograph of the prototype during the CERN beam tests.

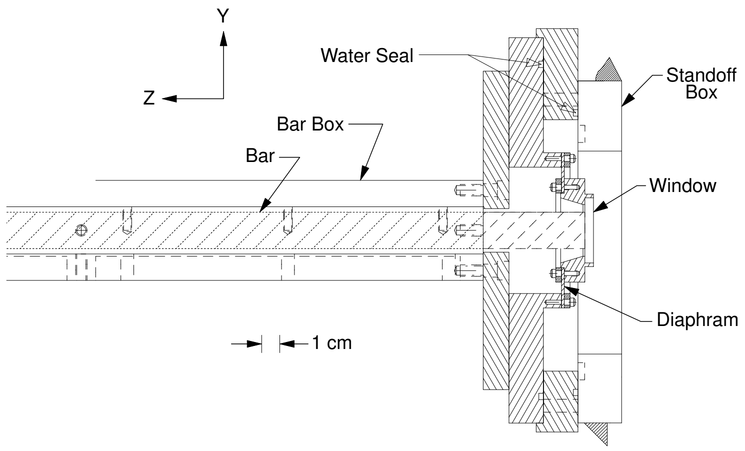

Figure 5: Bar coupling to the water-filled Standoff Box. The entrance window is glued to the end of the bar and sealed to the inner radius of a compliant annular diaphragm, whose outer radius is sealed to a flange that is bolted to the bar box and the Standoff Box.

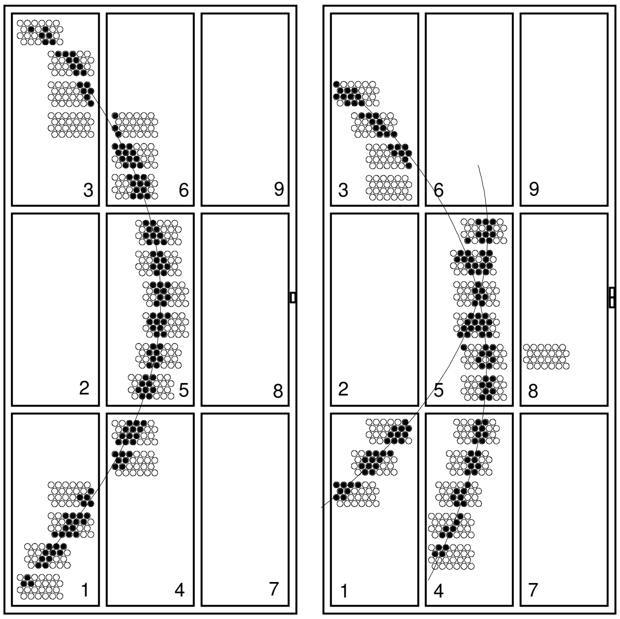

Figure 6: Two of the bundle configurations used for the tests. The PMTs with the highest occupancy for a large number of data events are shaded. The lines, which are the result of polynomial fits to the PMT occupancies, indicate the average position of the Čerenkov image in the detection plane. On the left : PMT arrangement for the configuration with $\theta_d = 20°$ and $\varphi = 0°$. The position of the quartz bar is indicated. On the right : PMT arrangement for the configuration with $\theta_d = 20°$ and $\varphi = 10°$. The positions of the two side-by-side quartz bars are indicated. To study backgrounds, some of the bundles were placed away from the expected position of the Čerenkov image, for instance the isolated bundle in window 8.

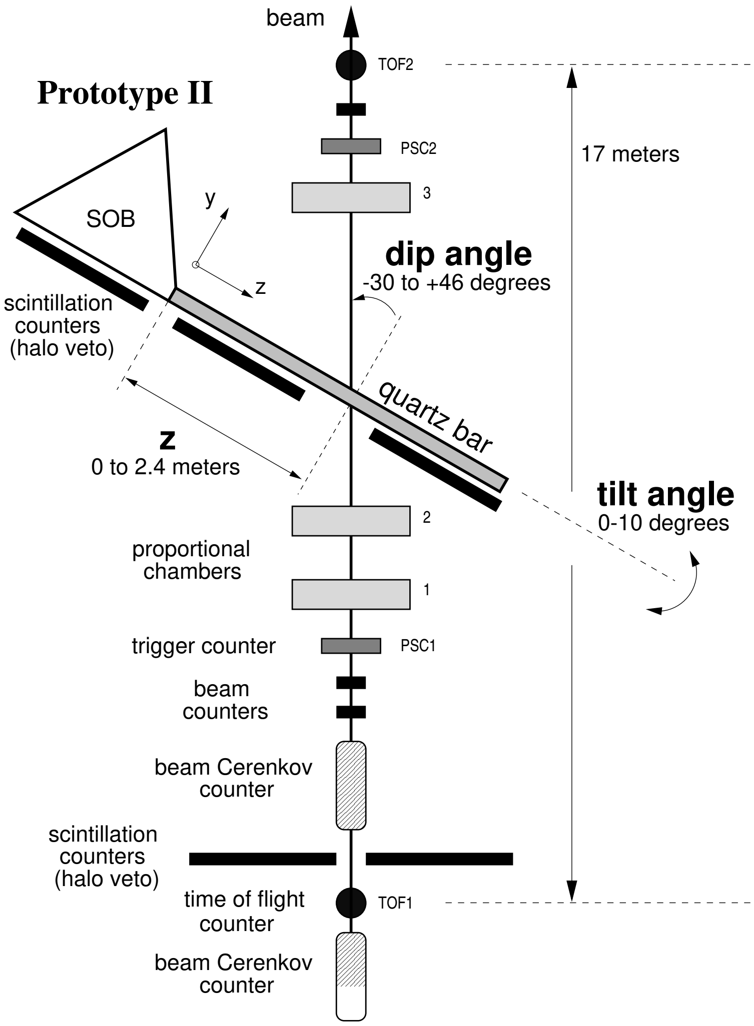

Figure 7: Top view (not to scale) of the T9 beam line at the CERN PS during the Prototype II tests.

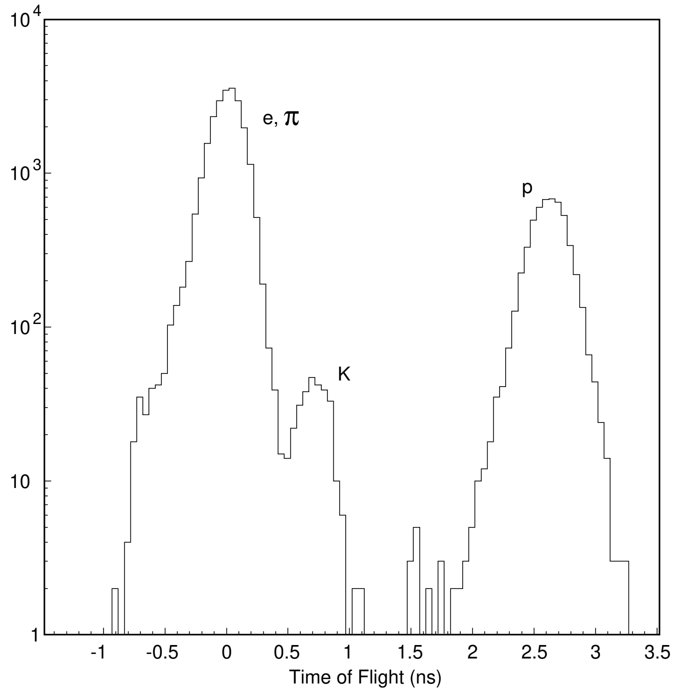

Figure 8: Time of flight of beam particles at 3 GeV/c momentum, with respect to $\beta = 1$ particles, as measured with the 17 m path TOF system.

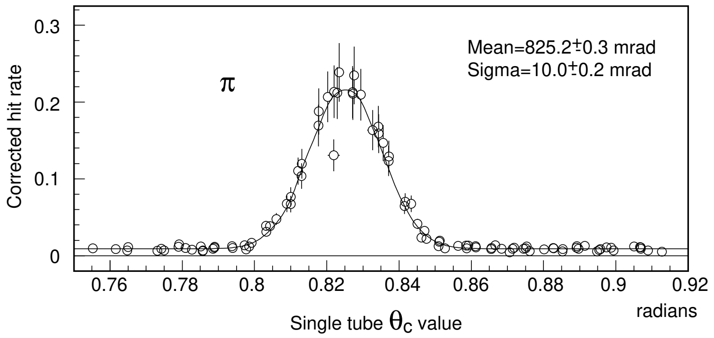

Figure 9: Čerenkov angle (θ_c) distribution of the hit rate for pions, fit to a Gaussian signal plus flat background. The fit result agrees well with the expected mean signal value of $\theta_c = 825.2\,\mathrm{mrad}$ for pions at $5.4\,\mathrm{GeV}/c$ momentum.

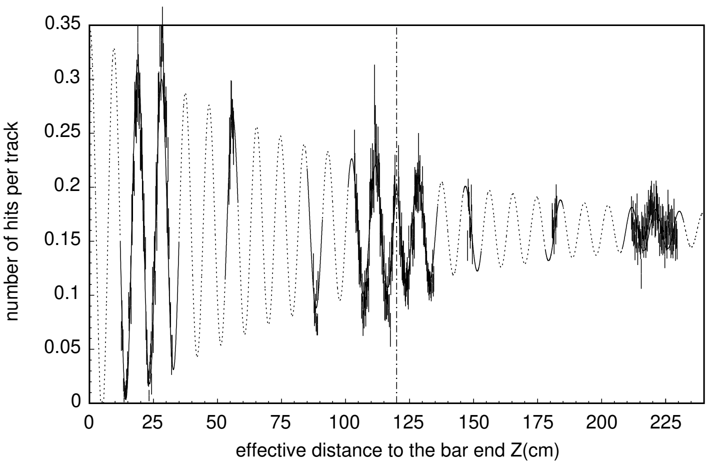

Figure 10: Number of hits per track for a tube on the Čerenkov image, as a function of the effective bar transmission distance Z, when the Standoff Box mirror is disabled. The dot-dashed line indicates the position of the bar-end mirror. The data are fit by an exponentially damped sine function, with a discontinuity at the mirror (dotted curve). The fit results of 9.25 cm for the period and 97 cm for the damping length are in good agreement with calculations for this tube position.

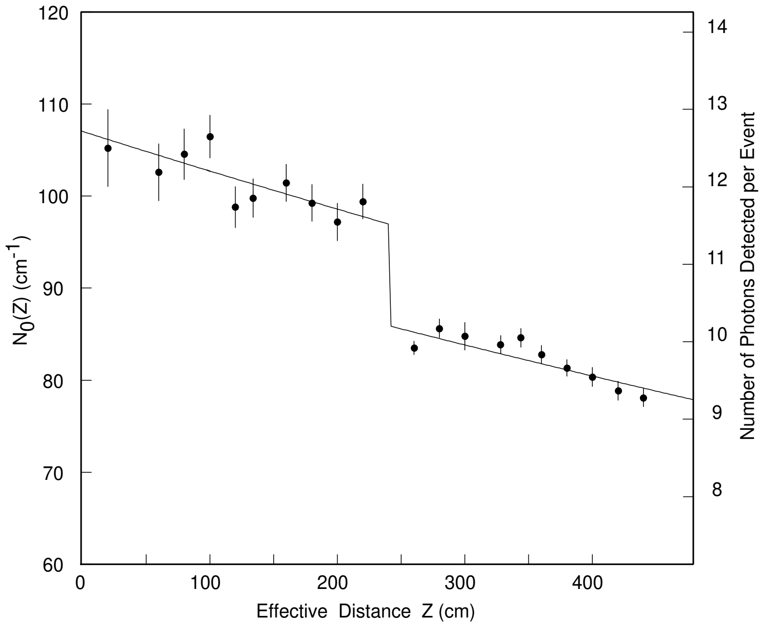

Figure 11: N_0 as a function of the effective bar transmission distance Z for the coarse Z scan at $\theta_d = \pm 20°$ and 5.4 GeV/c momentum. Pion and proton samples are averaged in the data points shown. The discontinuity at $Z = 240$ cm accounts for the end mirror reflectivity. A possible loss at the glue joint (for $Z = 120$ cm and $Z = 360$ cm) was not included in this fit. The scale at the right indicates the average number of signal photons extracted from a ring fit in the range $|\phi_c| < 1.0$ rad.

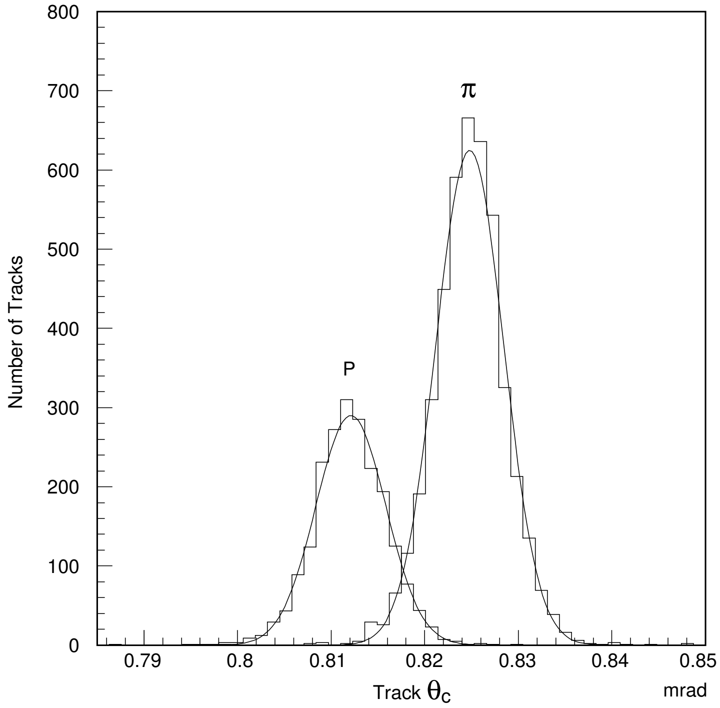

Figure 12: Čerenkov angle per track for pions and protons at 5.4 GeV/c, with $Z = 220$ cm.

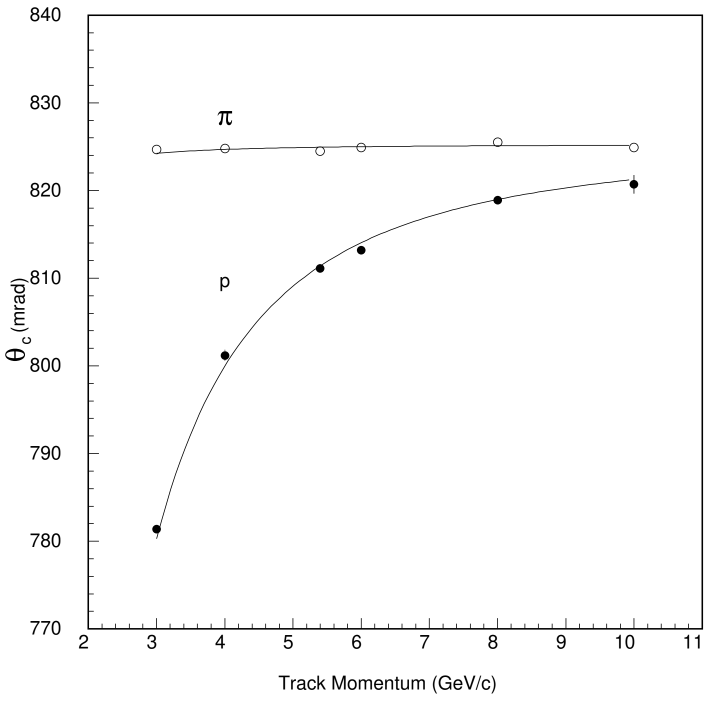

Figure 13: Average Čerenkov angle as a function of incident particle momentum (in GeV/c), for pions (open circles) and for protons (full circles). The result of a fit for the effective refractive index of the quartz is also shown.

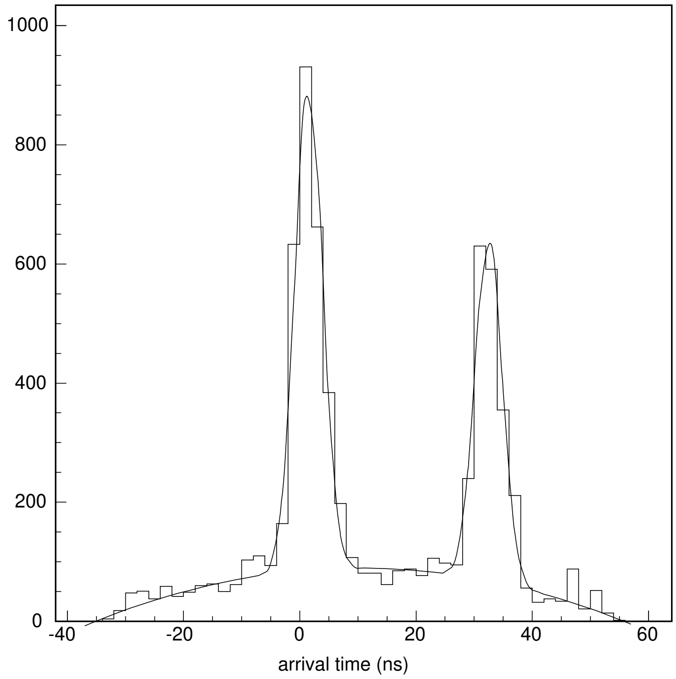

Figure 14: Arrival time of Čerenkov photons for a run at $\theta_d = 0°$, $z = 20\,\mathrm{cm}$, for $5.4\,\mathrm{GeV}/c$ pions. The time origin is taken at the interface between the quartz bar and the water. The peak at smaller time corresponds to direct photons, the one at larger time to reflected photons. The data are fit to two Gaussians plus a polynomial background.

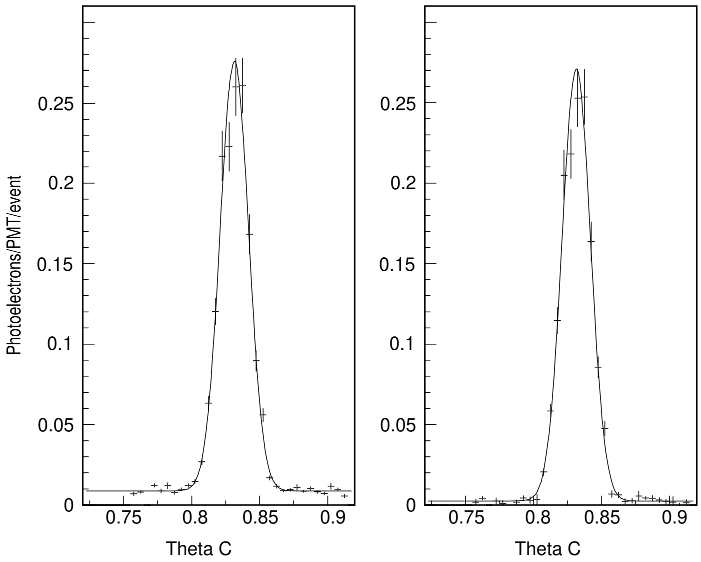

Figure 15: Hit rate θ_c distribution for 5.4 GeV/c pions at $\theta_d = 20°$. Both plots were corrected for random background by subtracting the random trigger hit rate. The distribution on the left was not corrected for beam-related background. The distribution on the right was corrected for beam-related background by subtracting the hit rate from a special run in which the beam missed the bar. The remaining background is associated with tracks generating the Čerenkov image.

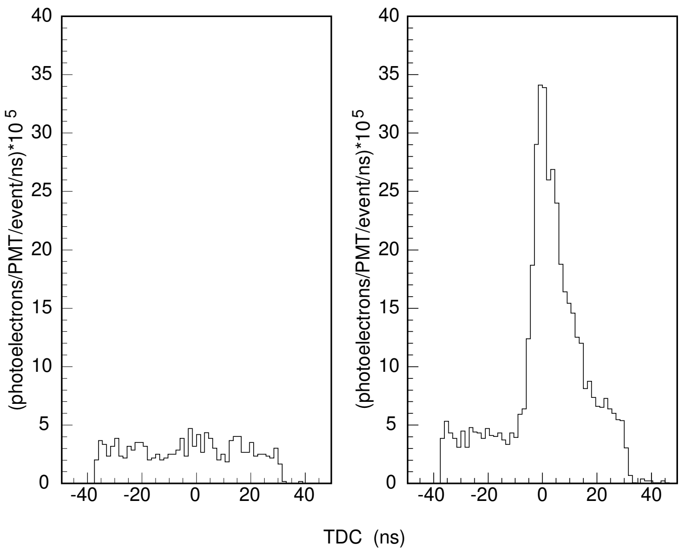

Figure 16: Timing signal for the tubes of a bundle located far away from the Čerenkov image, when the triggering particle does not cross the quartz bar (on the left side), and when it does (on the right side).